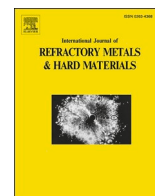




Contents lists available at ScienceDirect

# International Journal of Refractory Metals and Hard Materials

journal homepage: [www.elsevier.com/locate/IJRMHM](http://www.elsevier.com/locate/IJRMHM)

## Effect of WC-Co cermet positioning and NiCr interlayer on the microstructure and mechanical response of the dissimilar WC-Co / AISI 304 L rotary friction joint

Billel Cheniti<sup>a,\*</sup>, Brahim Belkessa<sup>a</sup>, Bouzid Maamache<sup>a</sup>, Naima Ouali<sup>a</sup>, Richard Sedlák<sup>b</sup>, Pavol Hvizdoš<sup>b</sup>, Zoheir Boutaghou<sup>a</sup>

<sup>a</sup> Research Center in Industrial Technologies CRTI, P.O. Box 64, Chéraga, Algeria

<sup>b</sup> Institute of Materials Research, Slovak Academy of Sciences, Watsonova 47, 04353 Kosice, Slovak Republic

### ARTICLE INFO

#### Keywords:

Rotary friction welding  
WC-Co cermet  
NiCr interlayer  
Interface  
Microstructure  
Mechanical properties

### ABSTRACT

In this work, incompatible properties of WC-Co cermet and AISI 304 steel were combined in the same component using rotary friction welding (RFW) process. The dissimilar joints were performed using a ductile NiCr interlayer with the change in the WC-Co cermet positioning i.e., fixed rotary side and feeding side. Similar microstructure across the weld joints was obtained of the different welding configurations that produced similar behavior in hardness and elastic modulus. A diffusion zone was formed at the weld interface as a result of the mutual inter-diffusion of both cermet (W and Co) and steel elements (Fe, Cr and Ni) that enhanced with the insertion of the interlayer when the cermet was fixed in rotary side. The introduction of the NiCr interlayer was beneficial to relax the residual stresses and improving the shear strength of the WC-Co cermet/AISI 304 L steel joints, which is promising technology for drilling tools industries.

### 1. Introduction

Joining WC-Co cermet to steel is combining the high hardness, wear and thermal resistance of the ceramic based-composite (WC-Co) to the tough and ductile steel [1]. In petroleum industry, the drill tool (drill bit) is often composed of two main parts: the steel body and the WC-Co cermet active part (bit). This later is joined to the former with brazing process using a soft Ag—Cu based alloy in order to avoid a brutal interface and insure properties gradient at the junction between the dissimilar materials [2,3]. The interfacial reaction between WC-Co cermet and a given filler material is dependent on the design of filler metal and the control of working temperature [4]. Several research works were conducted using various assembly processes to optimize the quality of this junction [5–8]. Among them, brazing technique using different heat sources such as: oxyacetylene fuel, electrical furnace and induction with various filler materials. This process is recommended to realize relatively strong and heat resistant drill-tool brazed joint with relatively low costs compared to other techniques [9]. However, it is argued that the obtained brazed joints cannot affront high mechanical resistance and high working temperatures [10]. Rotary friction welding

(RFW) process, known as the continuous drive friction welding method, exhibits the potential to be an effective alternative technique to join WC-Co to the steel body of the drill tool. The difficulty to produce defect free WC-Co/steel joint is mostly related to the large mismatch in thermal expansion coefficient (TEC) values between the base materials due to the different nature of chemical bonds for both materials that promotes the creation of cracks and other types of defects within the brazed joint [1,11]. Inserting an intermediate interlayer with TEC situated between those of the base materials is considered a suitable solution highly recommended to improve the joint strength by reducing the severe residual stresses induced by the heterogeneous heating during joining process. Various methods were reported in literature for depositing interlayer among which: nickel electroplated on Cu—Zn alloy that was sandwiched between the cermet and steel substrates [12]. Foils of Ag-Cu-Zn-Cd filler alloy placed between the WC-Co and the steel before brazing in furnace for various holding times [13]. Similar method was used by Avettand-Fènoël et al. [14] where the joining process was performed by flame brazing using four types of filler alloys. They found that using Cu-Zn-Ni braze improved the shear strength of the WC-Co/steel joint with the highest hardness and the formation of a diffusion layer at the boundary

\* Corresponding author.

E-mail address: [ch.billel@gmail.com](mailto:ch.billel@gmail.com) (B. Cheniti).

<https://doi.org/10.1016/j.ijrmhm.2021.105653>

Received 5 June 2021; Received in revised form 25 July 2021; Accepted 26 July 2021

Available online 31 July 2021

0263-4368/© 2021 Elsevier Ltd. All rights reserved.

of the cemented carbide. Powder metallurgy is frequently employed for manufacturing a functionally gradient materials by compacting Ni powder onto a pre-pressed WC-Co cermet then sintering the WC-Co/Ni compact in the vacuum furnace. This technique allows better densification of the compacts and avoids cracks formation at the interface due to the TEC mismatch of the two materials [7]. Chen et al. [12] highlighted the positive effect of Ni electroplated layer through the formation of intermetallic zones that enhance the bond strength of the WC-Co/interlayer/3Cr13 joints. Jiang et al. [15] demonstrated that the mechanical strengthen of the induction brazed WC-Co/carbon steel joint was influenced by  $\alpha$ -Cu and  $\beta$ -Cu phase distributed along the joint interfaces, while the high plastic deformation of the formed Cu–Zn interlayer along the WC-Co/braze interface, relieved the thermal residual stresses induced during brazing process. Similar results were found by Avettand-Fènoël et al. [16] who reported that the stress concentration at the brazed joint interface can be relieved by introducing Ni interlayer coated on the WC-Co cermet to form functionally gradient materials [17], or using an active filler metal with judicious chemical composition such as Ni–Cr, Ni–Cu, Ag–Cu–Zn and Ag-based filler alloy [2]. On the other side, it is believed that the thicker is the interlayer, the lower are the residual stresses in the brazed joint, due to the large volume available of the interlayer to be plastically deformed [18]. Conversely, Travessa et al. [19] reported, in the study conducted on Al<sub>2</sub>O<sub>3</sub>/304 steel joint, that the shear strength is much higher with 0.5 mm thickness of Ti interlayer compared to that with 1 mm thickness. Guo et al. [10] concluded that smooth surfaces with thin Ni-interlayer were favorable to produce high strength WC-Co/steel joints which was attributed to the combined effect of a bending component and the tensile residual stresses. Hence, a considerable attention should be paid to the limited effect of embedding an interlayer on the microstructure features, residual stresses and the mechanical behavior when designing a cermet/steel functionally graded material. In previous study [11], WC-Co cermet was successfully joined to 304 L stainless steel using RFW process. The optimal mechanical properties were obtained with 8 s friction time where the inter-diffusion of Co, Ni and Fe elements resulted in the formation of a new Cr-Co-Fe interlayer that increased the bonding

strength of the FSW joints. In the present work, interaction between NiCr interlayer, deposited on WC-Co cermet surface by oxyacetylene process, and the base materials in WC-Co/Ni-Cr/AISI 304 L joint using RFW process was investigated. Two welding configurations were considered i. e., WC-Co cermet fixed in rotary side (RS) and in feeding side (FS) and that with and without NiCr interlayer to evaluate their effect on the microstructure, micro-mechanical properties (hardness and Young's modulus) and bonding strength of the weld joints.

## 2. Material and methods

Cylindrical specimens of WC- 10 wt% Co cermet and AISI 304 stainless steel with similar 13 mm diameter and 12 and 40 mm length, respectively were used as base materials. Before welding operation, the specimen surfaces were mechanically grinded with P1000 grit SiC paper, to ensure an acceptable surface roughness and avoid interstitials and micro-voids that may alter the good junction, then ultrasonically cleaned in alcohol and dried. After that, the Ni–Cr interlayer was deposited on the WC-Co cermet by flame thermal spray process made by an oxyacetylene burner (mixture of acetylene and oxygen) using Na2B4O7 as Flux. as shown in Fig. 1a. The peak temperature, measured by SCANTEMP 490 non-contact infrared thermometer, reached during the deposition process is 900 °C, which is mainly below the decarburization temperature of the WC-Co cermet (above 1300 °C). It should be noticed that the interlayer thickness measured by optical microscope on the cross section of WC-Co cermet is about 300  $\mu$ m. The chemical compositions of the materials used in this study were given in Table 1. The welding operation was carried out by rapid rotary friction welding process using a friction welding machine (Fig. 1b), where the welding parameters were summarized in Table 2. Two different welding configurations were considered during the joining process: In first one, the WC-Co cermet was fixed in feeding side (FS) that allows moving only in the axial direction. In the second configuration, the WC-Co cermet was fixed in rotary side (RS) rotating at a constant velocity and that with and without NiCr interlayer. Thereafter, samples were cut perpendicularly to the weld interface and mechanically polished using standard techniques

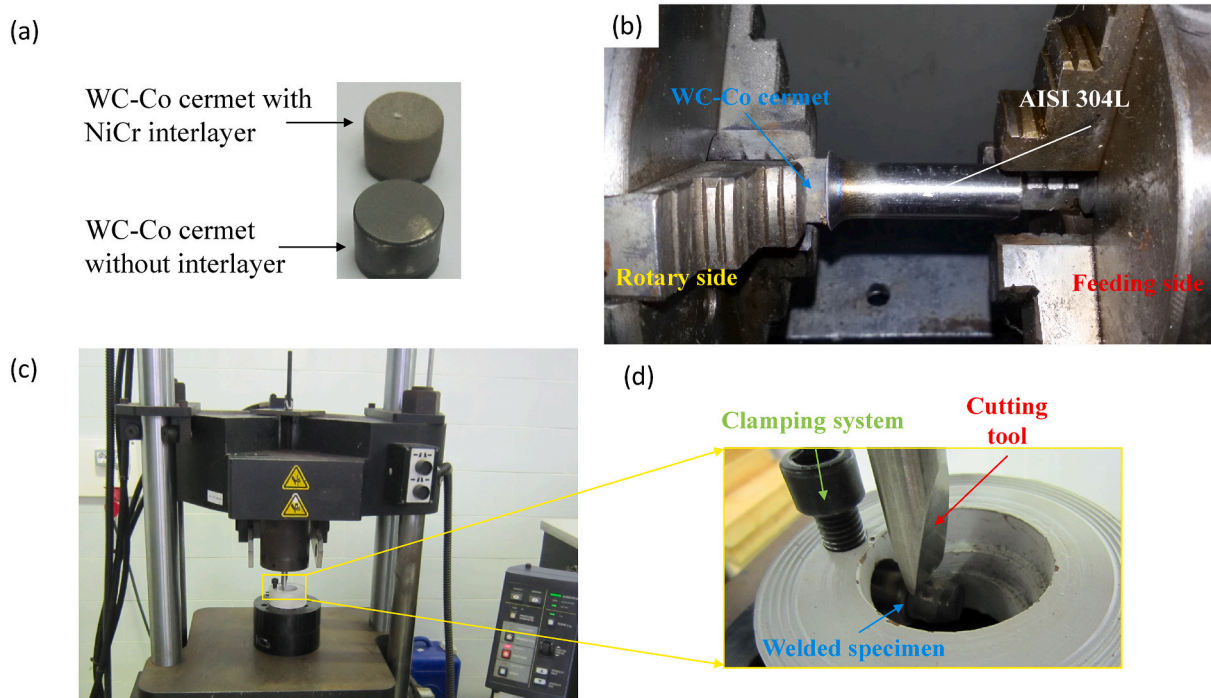


**Fig. 1.** (a): WC-Co cermet before RFW operation with and without NiCr-interlayer, (b): RFW operation with specimen's emplacement, (c): Bonding test using tensile machine (d): Instrument used to evaluate the bonding strength of the weld joints.

**Table 1**

Chemical composition of the materials used in this study.

| Elements (wt%)  | W  | C    | Co   | Ni   | Mn   | Cr   | Si  | Cu   | Mo   | Fe    |
|-----------------|----|------|------|------|------|------|-----|------|------|-------|
| WC-Co           | 77 | 11   | 10.5 | –    | –    | –    | 1.5 | –    | –    | –     |
| AISI 304 L ASS  | –  | 0,04 | –    | 8.2  | 1.25 | 18.3 | 0.3 | 0.33 | 0.26 | 71.32 |
| NiCr interlayer | –  | –    | –    | 32.5 | 5.1  | 23.2 | 1.2 | –    | 3.4  | 34.6  |

**Table 2**

Used friction welding parameters.

| Rotation speed (r/m) | Accosting time (sec.) | Friction pressure (MPa) | Friction time (s) | Upset pressure (MPa) | Upset time (s) |
|----------------------|-----------------------|-------------------------|-------------------|----------------------|----------------|
| 3000                 | 3.5                   | 3                       | 8                 | 5                    | 5              |

of metallographic preparation. The AISI 304 L steel was electrolytically etched using Struers LectroPol-5 machine working at 6 V for 10s with 1 M KOH solution. Afterwards, the microstructural examination was done by means of a Zeiss optical microscope and Zeiss AURIGA scanning electron microscope coupled with an energy dispersive spectroscope (EDS). X-ray diffraction (BRUKER D8 Discover instrument) was employed to detect the phases on different regions of the weld joints, operating at 40 V and 40 mA, using Co-K $\alpha$  (1.78897 Å) radiation with a large area detector (Vontec). The XRD measurements were focused on WC-Co cermet, the AISI 304 L steel and the WC-Co/304 L steel interface with a 0.5 mm incident beam using a video (Laser) camera system. The phases match was done by HighScore software with PDF4 database. The mechanical behavior of the welded specimens was investigated by hardness measurements along the welding interfaces using Vickers hardness testing machine (BUEHLER, Wilson VH3300) under 10 kgF load and a dwell time of 10 s. The local mechanical properties of the welding interface was conducted by nanoindentation measurements using an AGILENT G200 Nano-indenter machine with a Berkovich diamond indenter and maximum indentation depth of 700 nm. The hardness ( $H_{IT}$ ) and the Young's modulus ( $E_{IT}$ ) were automatically calculated

according to Oliver-Pharr method [20]. A special shear test was used to evaluate the bonding strength of the weld joints using an INSTRON machine as illustrated in Fig. 1c. The specimen's fixing and their loading mode were shown in Fig. 1d. Following the shear test, the fractured surfaces of the specimens were examined under the SEM.

### 3. Results and discussion

#### 3.1. Effect of WC-Co positioning and NiCr interlayer on the microstructural evolution of different zones in RF welds

The macrographic images of the cross section of the weld joints issued from different welding configurations are shown in Fig. 2(a–d). It is seen that all the weld interfaces (WI) exhibit a good metallurgical aspect without apparent defects such as voids or macro-cracks detected along the interfaces. Fixing the WC-Co cermet in FS results in small amount of weld flash (Fig. 2a and c), while important amount of flash is observed when the cermet is fixed in RS (Fig. 2b and d), which changes the physical appearance of the weld joints. As expected, the deformations are occurred in the AISI 304 L side of the joint suggesting its sufficient plastic flow compared to WC-Co cermet that does not participate in the weld flash formation. This behavior is explained by the high yield strength and high thermal conductivity of the cermet (300 GPa and 110 W m<sup>-1</sup> K<sup>-1</sup>, respectively) compared to the stainless steel ones (235 MPa and 16.2 W m<sup>-1</sup> K<sup>-1</sup>, respectively) that favor an asymmetric distribution of temperature during welding operation and consequentially high plastic deformation of the AISI 304 L steel during forging step. Hence, the axial shortening of the steel and the asymmetrical shape of the weld

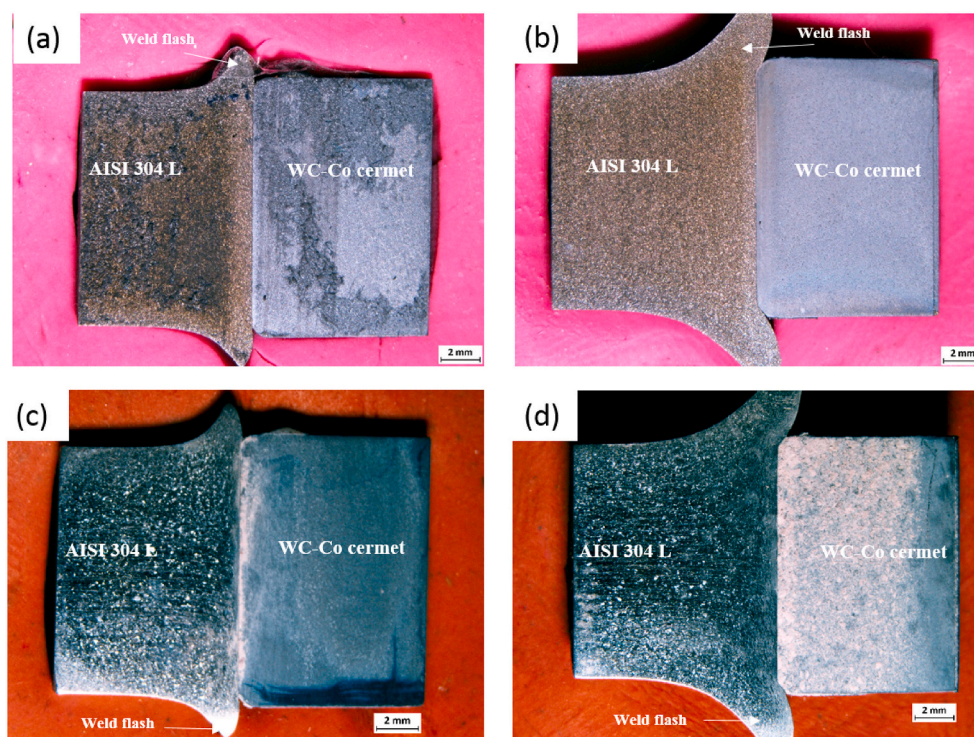


**Fig. 2.** Macrographic images of the as-welded friction joints: (a): WC-Co in FS WOI (b): WC-Co in RS WOI, (c): WC-Co in FS WI and (d): WC-Co in RS WI.

joint. The effect of WC-Co cermet positioning on the welds can be identified by the flash behavior (aspect). It can be seen that fixing the WC-Co cermet in FS (Fig. 2a and c), the flash is slightly oriented towards outside. However, the WC-Co cermet is incised into the steel with important amount of flash obtained when the cermet is positioned in RS (Fig. 2c and d). On the other side, no apparent changes are observed with the introduction of NiCr interlayer and that for both welding configuration (WC-Co fixed in FS and RS).

The microstructures of the AISI 304 L steel from the base metal (BM) to the WI of the specimen with NiCr interlayer fixed in RS are shown in Fig. 3(a–d). The BM consists of austenitic grain structure of 40  $\mu\text{m}$  main grain size with some annealing twins within the microstructure (Fig. 3a).  $\delta$ -ferrite (dark dots) is detected throughout the BM grains that decreases with approaching the WI. The heat-affected zone (HAZ) exhibits coarse grains (Fig. 3b) with no deformation due to the excessive heat generated during friction operation. In the thermo-mechanically affected zone (TMAZ), the grains are partially recrystallized and elongated following the materials flow with small grain size,  $\sim 25 \mu\text{m}$ , compared to those in BM and HAZ (Fig. 3c), as a consequence of the severe plastic deformation induced by the forge pressure at high temperature. Remarkable grain refinement is occurred at the WI for the 304 L steel side (Fig. 3d) from the continuous dynamic recrystallization of austenitic grains (dynamic recrystallized zone), as a result of the combine effect of high working temperature (950  $^{\circ}\text{C}$ ) and severe plastic deformation of the upset force, which results in improvement of the mechanical properties in this zone [21]. It is worth mentioning that the ferrite phase in this zone is barely detected with small fraction (0.5%), which is significantly lower than that in the BM and the TMAZ (5% and 3%, respectively). As mentioned above, the high thermal conductivity of WC-Co cermet compared to the 304 L stainless steel one allows to the former to have a cooling effect on the stainless steel, which results in the decrease of peak temperature (950  $^{\circ}\text{C}$ ) at the WI during welding process (below the temperature of  $\delta$ -ferrite formation that is 1150  $^{\circ}\text{C}$ ). Hence, no new high-temperature  $\delta$ -ferrite is formed during friction process in the DRZ. Similar results were found by Ma et al. [22] who noticed the formation of  $\delta$ -ferrite free zone near the WI whereas Bhamji et al. [23] demonstrated that the shorter the exposure time to high temperature, the

weaker the chances to  $\delta$ -ferrite formation at the WI in 316L linear friction welds.

The cross section microstructure at the vicinity of the WC-Co cermet/AISI 304 L steel interface in the sample with NiCr interlayer is displayed in Fig. 3e. High magnification on the WI obtained using SEM revealed 40  $\mu\text{m}$  thickness of the NiCr interlayer, in the center of the WI, that consists of white islands (A) distributed throughout a dark matrix (B). According to the EDS point analysis conducted in these two regions (Table 3), the dark phase B may be solid solution of Fe-Ni-Co and the white islands A are chromium-rich (W–Cr)C solid solution as a consequence of the high solubility limit of Cr in hexagonal WC structure (5–7 wt%) [24]. Fig. 4a and b show the WC-Co/AISI 304 L interface of the specimens with and without NiCr interlayer, respectively. It is clear to see the good metallurgical bonding in the joint with NiCr interlayer with three distinguished regions, the WC-Co cermet (dark grey), AISI 304 L steel (bright region) and the NiCr interlayer with light grey that overlaps the steel and the cermet. This aspect suggests an eventual formation of inter-diffusion zones between the interlayer and the base materials. On the other side, important continuous micro-cracks along the WC-Co/AISI 304 L interface are detected in the specimen without NiCr interlayer (of about 45  $\mu\text{m}$  diameter) compared to small fine cracks (5  $\mu\text{m}$  diameter) in the sample with NiCr interlayer, mainly propagated in the center of the WI through the NiCr interlayer. Based on Fig. 4a and b, the presence of these cracks at the WI reflects the poor bonding between the cermet and the steel in the specimen without NiCr interlayer. This can be attributed to the relatively small plastic deformation of the cermet at the bonding interface compared to the steel, due to the large difference between their TEC ( $5 \times 10^{-6} \text{ K}^{-1}$  for the WC-Co cermet and  $12 \times 10^{-6} \text{ K}^{-1}$  for the 304 L steel) [25,26], resulting in strong residual stresses near the bonding interface [27]. Consequently, the formation of cracks along

**Table 3**  
EDS point analysis of the two regions (A and B) of the NiCr interlayer.

| Elements Wt% | W     | Co   | Ni    | Cr    | Fe    | Mo   | Mn   |
|--------------|-------|------|-------|-------|-------|------|------|
| A            | 13.24 | 5.25 | 4.67  | 32.87 | 36.51 | 2.55 | 4.91 |
| B            | 6.01  | 8.36 | 20.89 | 21.79 | 27.58 | 1.38 | 3.98 |

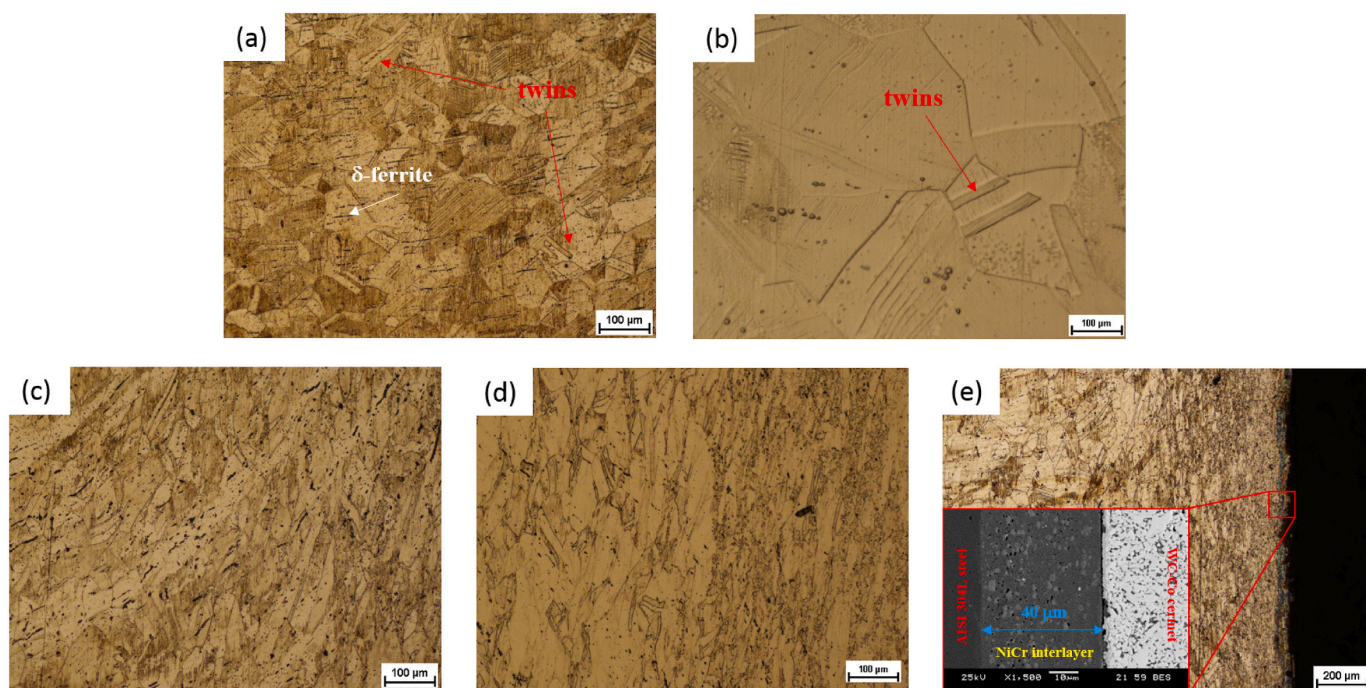


**Fig. 3.** Micrographs of different regions in the 304 L steel side of the weld joint RS-WI: (a): BM (b): WC-Co cermet/ AISI 304 L interface with SEM zoom view on NiCr interlayer (c): HAZ (d): TMAZ and (e): DRZ.

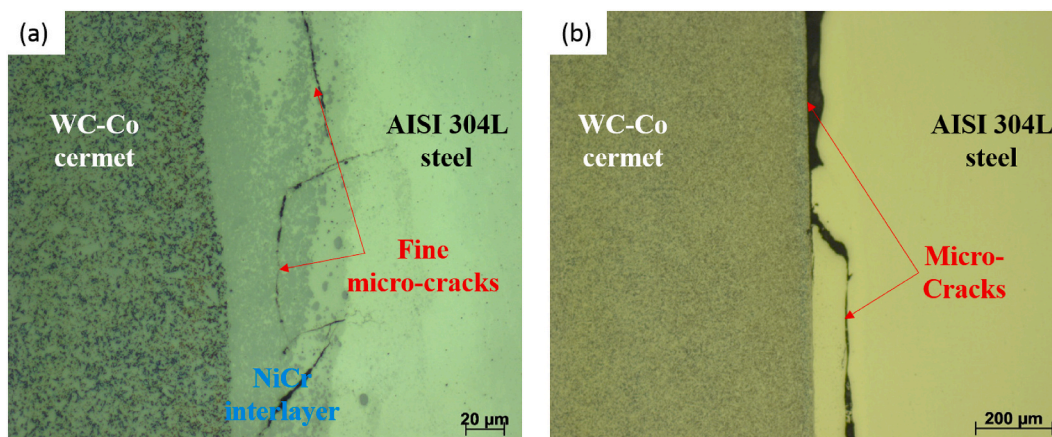


Fig. 4. Optical micrographs of the WC-Co/AISI 304 steel interface, (a): specimen with NiCr interlayer and (b) specimen without interlayer.

the WI with a lack of surface's contact between the base materials during welding operation, suggests that the WC-Co/AISI 304 L interface is the weakest part of the weld joint. However, the introduction of NiCr interlayer with intermediate TEC ( $9.7 \times 10^{-6} \text{ K}^{-1}$ ) [24], leads to less stress concentration at the WC-Co/AISI 304 L interface due to the gradient structure [17]. Besides, regardless the WC-Co positioning (RS or FS), the NiCr interlayer thickness is found to be the smallest in the center of the WI (around 50  $\mu\text{m}$ ) and increases with approaching the edges (periphery) as illustrated in Fig. 5a and b. This phenomenon is explained by the plastic deformation generated during the friction process that causes an important materials flow (mainly NiCr and stainless steel) towards the peripheral region of the welds.

Fig. 6a and b show the EDS profiles analysis conducted across the WC-Co/AISI 304 L steel interface in the samples without NiCr interlayer. Similar behavior is observed wherever the WC-Co cermet is positioned i. e., RS or FS. Remarkable microstructural changes on the WC-Co cermet aspect at the vicinity of the WI are clearly observed, where the WC particles appeared severely deformed (sharpless edges) with dark grey compared to the light grey WC particles in the WC-Co cermet base material. As seen in Fig. 6a and in addition to Fe element, Ni and Cr diffuse from the stainless steel to the inside of the WC-Co cermet, as well as the main alloying elements of the 304 L stainless steel. Furthermore, the Fe atoms diffuse to a great extent from the stainless steel towards the WC-Co cermet side (Fig. 6b) and penetrate the cermet structure, which may enhance the ductility of the WI. Simultaneously, the concentration gradient of the W element towards the WI with the decrease trend of C concentration and the increase of the Co element suggest more likely the formation of  $\eta$  ( $\text{Co}_2\text{W}_4\text{C}$ ) phase due to the decarburization of WC particles under the plastic deformation at high temperature at the WI, as depicted in Fig. 6a and b. This presumption is confirmed by the XRD

conducted on the WC-Co/AISI 304 L interface where  $\text{Co}_2\text{W}_4\text{C}$  phase is detected as shown in Fig. 7, which is in good agreement with the results found by Chen et al. [7] on the WC-Co/stainless steel diffusion brazed joint. It is worth mentioning that the high solubility limit of Ni into the W structure favors the diffusion of elements across the WI and results in the formation of inter-diffusion zone (mainly  $\eta$  phase, Fe-Ni-W and W-Ni solid solutions) according to W-C-Ni and Fe-Ni-WC phase diagrams [28,29] that may contributes to the intimate bonding of the welded joints.

The areal distribution of elements at the WI in the sample with NiCr interlayer is shown in Fig. 8a. As it can be seen, an inter-diffusion zone is formed between the NiCr interlayer and the cermet that mainly consists of Ni, Cr and Co elements. The EDS line scanning analysis conducted across the WC-Co/NiCr interlayer illustrated in Fig. 8b revealed that Fe, Ni and Cr elements reduce continuously from the interlayer towards the cermet with an important concentration of Ni element along the interface with the WC-Co cermet (Fig. 8a). Meantime, the W and Co elements decrease gradually towards the interlayer with a high concentration of Co element penetrated into the interlayer and found at the interface with the cermet (Fig. 8a). Since its high chemical affinity to Ni, Co element showed a solubility limit of 12% in Ni matrix at high temperature that promotes the formation of Co-Ni solid solution oversaturated in Ni element, which is confirmed by the results found by Avettand-Fènoël et al. [16]. This diffusion activity of Ni, Cr, Co and W elements through the WI resulted from the mutual solubility between Ni-Co, Ni-W and Cr-W according to their binary phase diagrams, suggests the formation of a gradient structure as a functionally graded material with gradient mechanical properties, which may enhance the intimate bonding between the dissimilar welded materials. Furthermore, it can be concluded that the introduction of NiCr interlayer inhibits the  $\eta$  phase formation

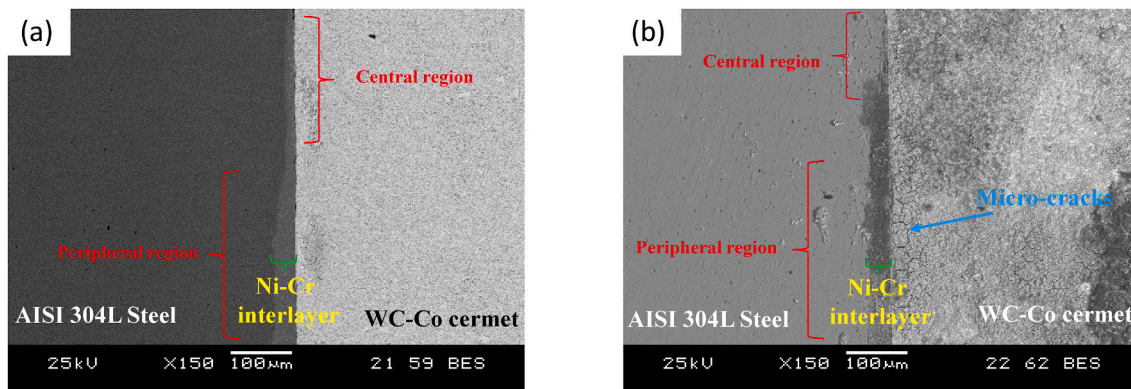


Fig. 5. SEM micrographs of WC-Co cermet/NiCr/AISI 304 interface obtained when WC-Co cermet is fixed in: (a): feeding side and (b) rotary side.

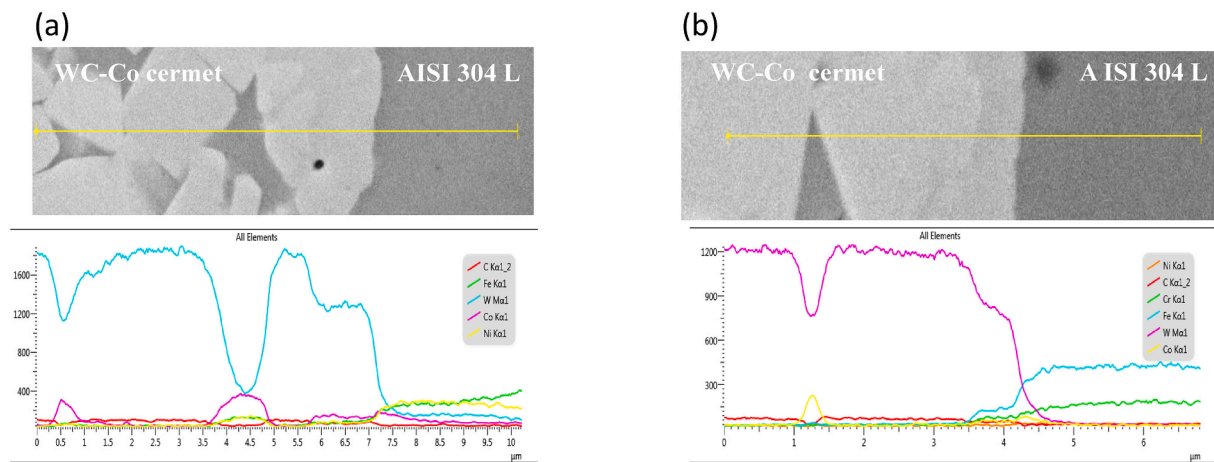


Fig. 6. SEM images and EDS line analysis of WC-Co cermet/AISI 304 interface obtained when WC-Co cermet is fixed in: (a): Feeding side and (b) rotary side.

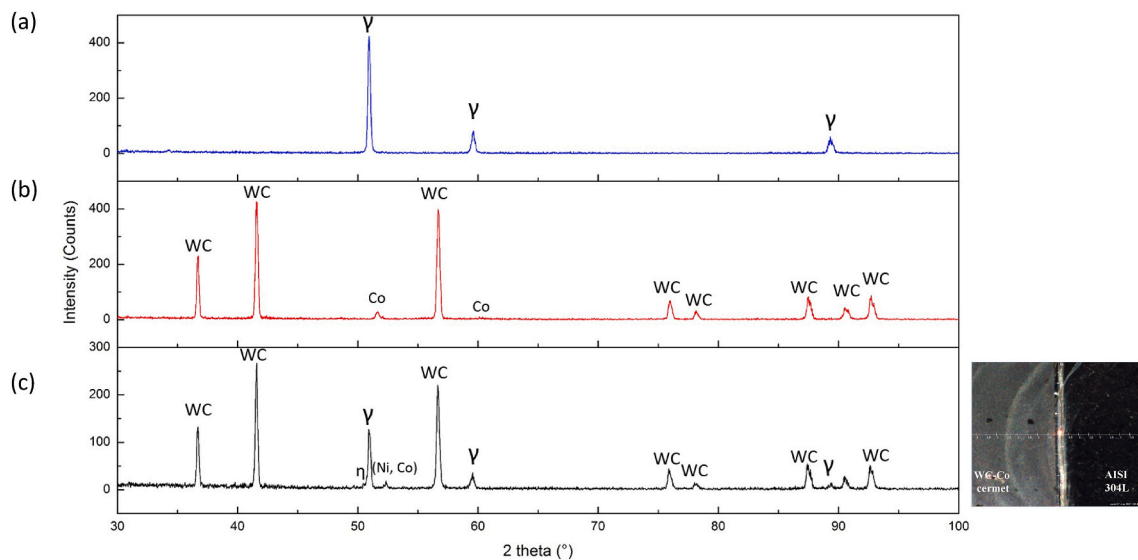


Fig. 7. XRD patterns: (a) 304 L steel base metal, (b) WC-Co cermet base material and (c): WC-Co/cermet/AISI 304 L interface without NiCr interlayer with the corresponding measurement location.

and leads to Co–Ni solid solution rather than undesirable phases.

### 3.2. Mechanical behavior of RF welds

#### 3.2.1. Global and local mechanical properties across the rotary friction joints

The hardness profiles across the RF welds issued from different welding configurations are shown in Fig. 9. An average value of three measurements is considered with respect to the three levels of the welded joint (top, middle and bottom for P1, P2 and P3, respectively) as illustrated in Fig. 9. All the weld joints exhibit a similar tendency where the lowest hardness values are recorded in the steel side (250 HV) and the highest ones are in the WC-Co cermet with 1520 HV. It can be seen that regardless the WC-Co cermet positioning, a steep increase in hardness is observed as moving through the WI whereas a gradual increase in hardness values is recorded at the WI in the samples with NiCr interlayer. The inter-diffusion of the interlayer elements (Ni and Cr) towards the cermet and the changes in the WC-Co cermet structure close to the WI resulted from its decomposition into Co and W elements, justify the continuous increase in hardness across the WI and explain the intermediate hardness value (950 HV) recorded in the interlayer. These results are similar to those found by Amirasiri et al. [30], where the

diffusion of Ni towards the base alloys and the formation of intermetallic and solid solutions enhanced the hardness at the interface by increasing bonding time in WC-Co/AISI 4145 steel diffusion brazed joint. However, Avettand-Fènoël et al. [16] observed that the formation of Co–Ni solid solution promoted an increase in hardness between the steel and the WC-Co cermet that increased with Ni interlayer thickness (up to 0.1 mm), which avoided the formation of the  $\eta$  brittle phase at the steel-cermet interface. For the better understanding of the mechanical response of each zone of the weld joints, hardness ( $H_{IT}$ ) and Young's modulus ( $E_{IT}$ ) evolution along the WI are established using nano-indentation measurements as shown in Fig. 10(a–c). From the load-displacement curves (Fig. 10a), the WC-Co cermet exhibits the highest applied load for the same penetration depth followed by the NiCr interlayer then the AISI 304 L steel where the lowest load is recorded. In the steel side (Fig. 10b and c), the DRZ shows the highest hardness ( $H_{IT}$ ) compared to the TMAZ while the lowest one is obtained in the HAZ. This behavior is related to the microstructure of the individual zone where the fine-recrystallized grains are responsible on the increase in hardness values (Table 4) of the DRZ (Hall-Patch effect). On the other side, all the zones exhibit similar values of elastic modulus where the highest value is obtained in the DRZ as shown in Fig. 10c. Meantime, the highly deformed grains with important mechanical stresses in the TMAZ allow

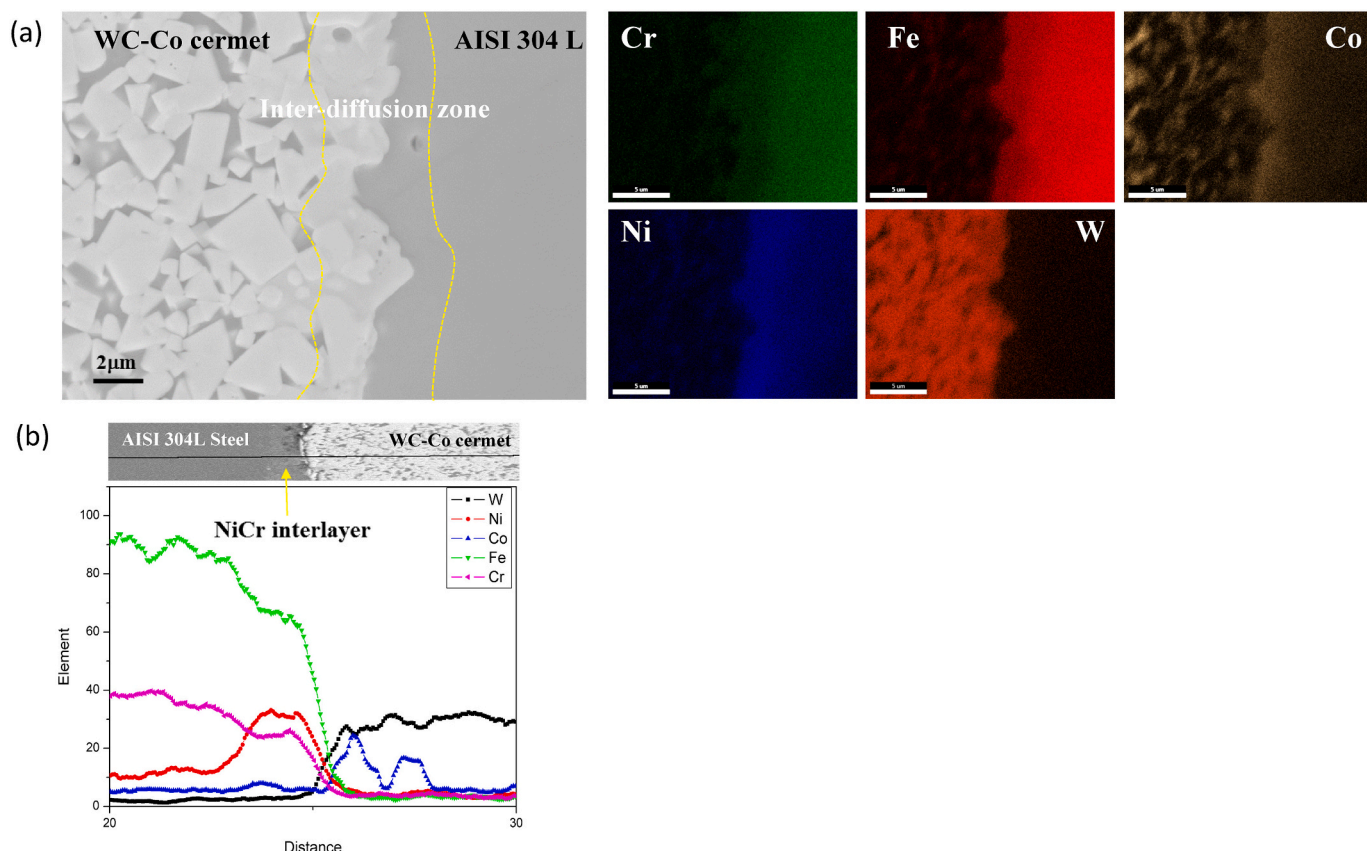


Fig. 8. (a): SEM image with the corresponding compositional EDS maps of the WC-Co cermet/AISI 304 interface with interlayer obtained when WC-Co is fixed in RS and (b) EDS line analysis across the WC-Co/AISI 304 L interface with NiCr interlayer.

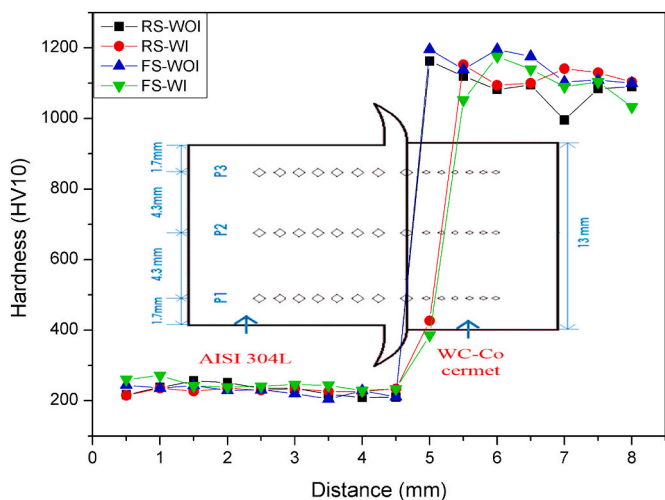


Fig. 9. Vickers hardness profiles of WC-Co cermet/304 L friction joints.

the improvement of the mechanical properties of this zone with respect to the coarse un-deformed grains of the HAZ as displayed in Table 4. In addition, measurements conducted on the flash area reveal average values of  $H_{IT}$  and  $E_{IT}$  ( $5.6 \pm 0.2$  GPa and  $220 \pm 9$  GPa, respectively) roughly similar to those recorded in the DRZ ( $5.9 \pm 0.1$  GPa and  $225 \pm 7$  GPa) despite the distinguished microstructure among these zones.

### 3.2.2. Bonding strength and fractured surfaces

The strength values resulted from the special shear test carried out on the different RF welds are resumed in Table 5. It can be observed that the

shear strength depends strongly on the NiCr interlayer presence. The maximum strength value ( $523 \pm 8$  MPa) is obtained on the joint with NiCr interlayer when the WC-Co is fixed in RS, whereas fixing the cermet in AS without interlayer results in the lowest strength value ( $475 \pm 7$  MPa). Considering the cermet positioning, it is known that the plastic deformations induced by the forging process can break the oxide films of the base materials surface, which may accelerate the inter-diffusion of elements across the WI. However, a small increase in strength ( $481 \pm 5$  MPa) is obtained when fixing the WC-Co cermet in RS compared to that in FS, despite the relatively important plastic deformations (important weld flash) observed in the former joint. Hence, a limited contribution to improve the strength in the WC-Co/AISI 304 L joint is obtained when fixing the cermet in RS. On the other side, a clear enhancement of shear strength is obtained with the introduction of the NiCr interlayer. This behavior can be explained as follows: Firstly, the NiCr with intermediate TEC reduces the mismatch in the TECs of the base materials, which relaxes and reduces the thermal stresses in the WI. Secondly, the excellent plasticity behavior of NiCr interlayer allows a small amount of residual stresses to reach the base materials, while the important stresses are dissipated by the plastic deformation of the interlayer [7]. Finally, the high diffusion rate of Ni, Co and Cr elements with the creation of inter-diffusion zone at the WI increase the contact area and lead to more effective bonded joint [17].

The fractured surfaces of the welded joints issued from special shear tests are shown in Fig. 11(a-d). The fractographs of the WC-Co/AISI 304 L steel joint without NiCr interlayer (Fig. 11a and b) exhibit a typical brittle fracture mechanism due to the inherent fragility of the WI. It can be seen on Fig. 11b the WC particles severely deformed due to the forging forces applied during friction welding process. As expected, the fracture occurrence on the WC-Co/AISI 304 steel interface suggests that the interface is the weakest part of the RF joints without interlayer and

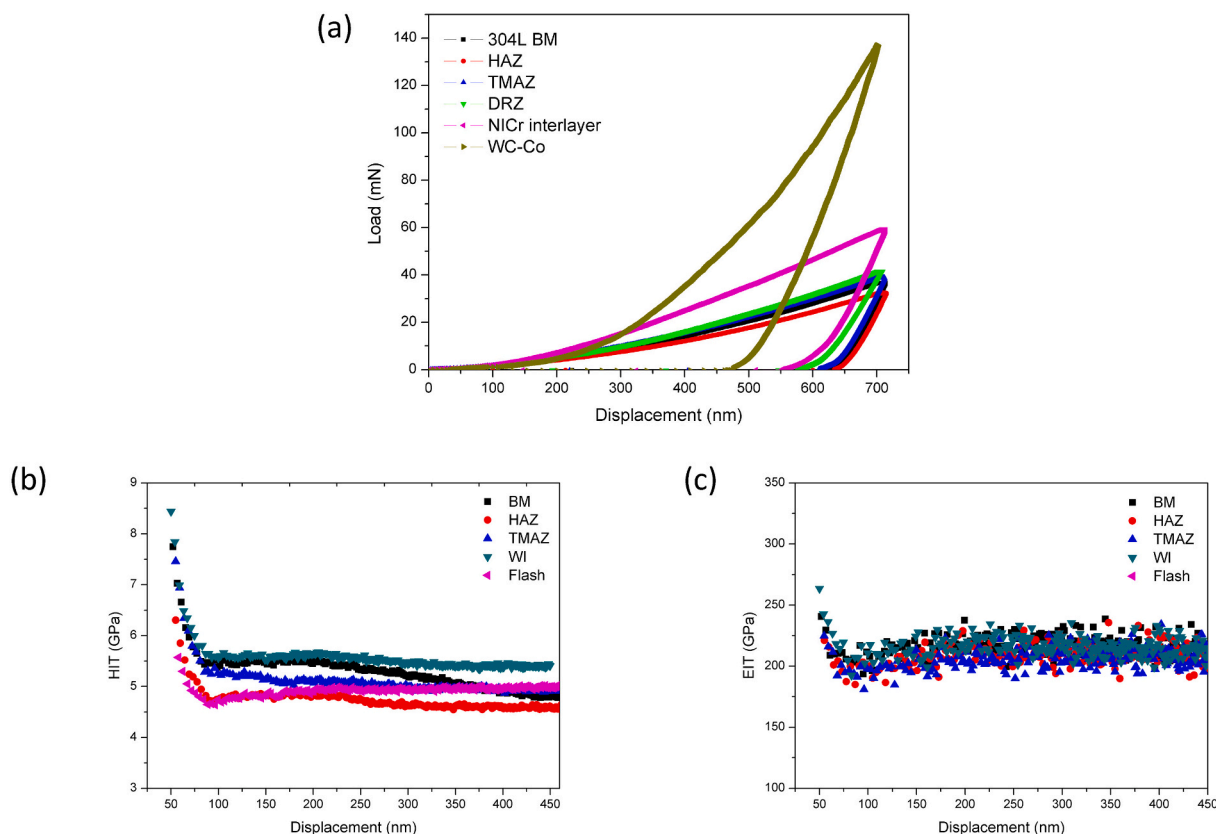


Fig. 10. Load-displacement curves of the different regions in the WC-Co/AISI 304 L steel joints (b): Hardness ( $H_{IT}$ ) and (c) Elastic modulus ( $E_{IT}$ ) distribution in the different regions in the steel side.

Table 4

Hardness ( $H_{IT}$ ) and elastic modulus ( $E_{IT}$ ) values of the different zones issued from WC-Co cermet/NiCr/AISI 304 L steel joint fixed in RS.

|                | 304 L BM      | HAZ           | TMAZ          | DRZ           | Flash         | NiCr interlayer | WC-Co cermet   |
|----------------|---------------|---------------|---------------|---------------|---------------|-----------------|----------------|
| $H_{IT}$ (GPa) | $4.2 \pm 0.3$ | $3.6 \pm 0.4$ | $4.7 \pm 0.2$ | $5.9 \pm 0.1$ | $5.6 \pm 0.2$ | $7.4 \pm 0.4$   | $26.1 \pm 0.5$ |
| $E_{IT}$ (GPa) | $198 \pm 5$   | $181 \pm 3$   | $216 \pm 4$   | $225 \pm 7$   | $220 \pm 9$   | $237 \pm 3$     | $512 \pm 11$   |

Table 5

Shear strength value of the different rotary friction welds.

|                      | Without NiCr interlayer |             | With NiCr interlayer |             |
|----------------------|-------------------------|-------------|----------------------|-------------|
|                      | WC-Co in FS             | WC-Co in RS | WC-Co in FS          | WC-Co in RS |
| Shear strength (MPa) | $475 \pm 7$             | $481 \pm 5$ | $514 \pm 9$          | $523 \pm 8$ |

that despite the element diffusion already observed across the WI. The formation of brittle  $\eta$  phase and the high concentration of residual stresses in the WI resulted from the large gap in TEC between the WC-Co cermet and the stainless steel are the main reason of the fracture occurrence in this region. The SEM photographs (Fig. 11c–e) and the EDS analysis (Fig. 11f) of the fractured surface of both joints with NiCr interlayer (RS and FS) show that the fracture has taken place through the interlayer, close to the WC-Co cermet, since the main elements detected are W, Co Ni and Cr. A dimple fracture mode (ductile mechanism) is shown on the fractured surfaces (Fig. 11e), this behavior is explained by the high plastic deformation of NiCr interlayer that release the residual stresses formed in the WC-Co cermet/AISI 304 L interface during welding process. Hence, it can be concluded that the introduction of NiCr interlayer relaxes the structure between the cermet and the steel and improves the metallurgical bonding of the friction-welded joints by

enhancing the inter-diffusion of elements through the WI.

#### 4. Conclusion

In this work, the comparing investigation between the WC-Co/AISI 304 L steel rotary friction joints with and without NiCr interlayer and the effect of the cermet positioning were experimentally studied.

- The mutual inter-diffusion of both WC-Co cermet and steel elements resulted in the creation of new regions at the weld interface where the diffusional process was promoted with the NiCr interlayer presence.
- The introduction of NiCr interlayer promoted the Co–Ni solid solution formation, enhanced the inter-diffusion of elements through the WI and inhibited the brittle  $\eta$  phase formation.
- The nanoindentation measurements revealed that the highest hardness was obtained in the DRZ, while no change in the elastic modulus values was noticed from the different regions in the steel side. Simultaneously, intermediate values of hardness and Young's modulus were recorded in the NiCr interlayer, which possessed positive effect of the bonding strength of the friction joints.
- The maximum shear strength value (512 MPa) was obtained in the RF joint with NiCr interlayer and the WC-Co cermet was fixed in RS, where the ductile fracture was occurred through the interlayer. Whereas, a fragile fracture had taken place near the weld interface in

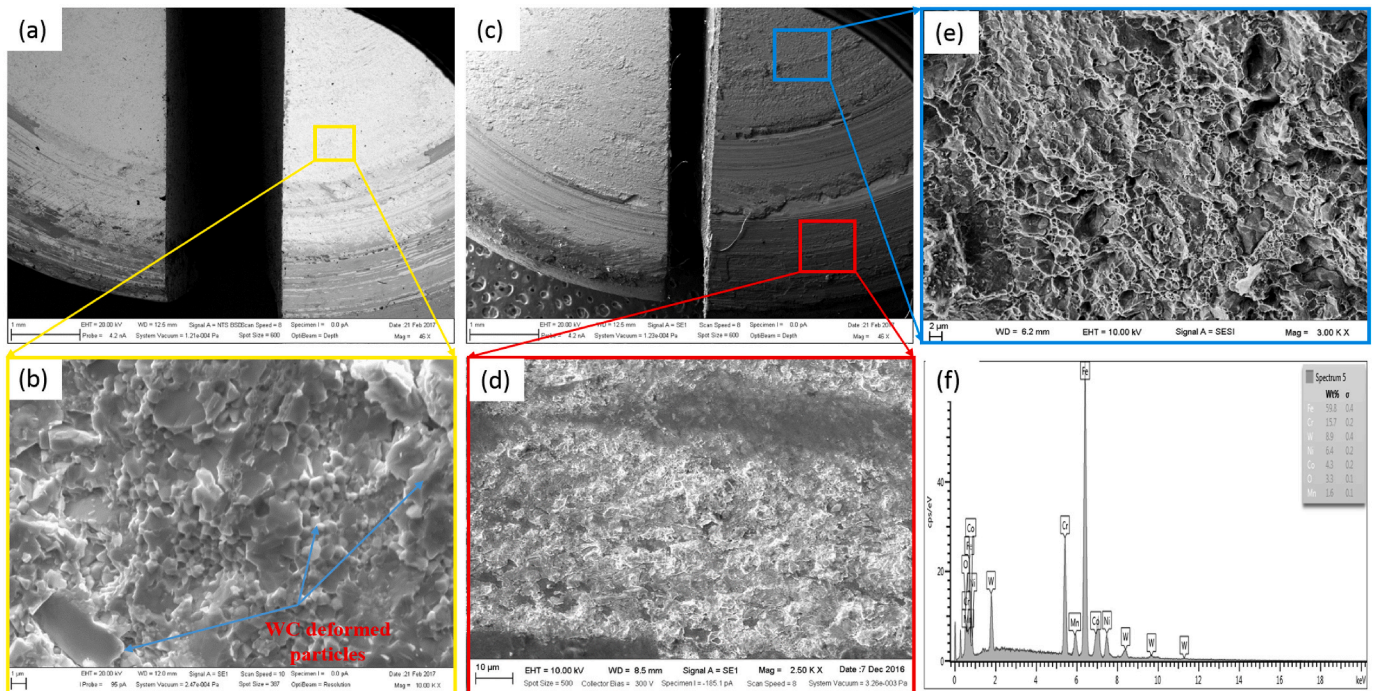


Fig. 11. SEM fractographs with magnified view of the fractured surface obtained in: (a-b) WC-Co/AISI 304 L steel joint without interlayer, (c-e) WC-Co cermet/AISI 304 L steel with NiCr interlayer and (f): EDS analysis conducted in the fractured surface in Fig. 11d.

the RF joint where the WC-Co cermet was fixed in FS without NiCr interlayer.

#### Authorship statement

All persons who meet authorship criteria are listed as authors, and all authors certify that they have participated sufficiently in the work to take public responsibility for the content, including participation in the concept, design, analysis, writing, or revision of the manuscript. Furthermore, each author certifies that this material or similar material has not been and will not be submitted to or published in any other publication before its appearance in The International Journal of Refractory Metals and Hard Materials.

#### Declaration of Competing Interest

The authors declare that they have no known competing financial interests or personal relationships that could have appeared to influence the work reported in this paper.

#### Acknowledgments

The authors would like to thank Mr. Oussama Benstira, Mr. Jabbar Hassan Ammar for the welding machine access. Also gratefully acknowledge the sponsorship from APVV-18-0438 project and l'Entreprise Nationale de Services aux Puits (ENSP-Sonatrach).

#### References

- [1] M.N. Avettand-Fènoël, T. Nagaoka, H. Fujii, R. Taillard, Characterization of WC/12Co cermet-steel dissimilar friction stir welds, *J. Manuf. Process.* 31 (2018) 139–155, <https://doi.org/10.1016/j.jmapro.2017.11.012>.
- [2] B. Cheniti, D. Miroud, R. Badji, D. Allou, T. Csanádi, M. Fides, P. Hvizdoš, Effect of brazing current on microstructure and mechanical behavior of WC-Co/AISI 1020 steel TIG brazed joint, *Int. J. Refract. Met. Hard Mater.* 64 (2017) 210–218, <https://doi.org/10.1016/j.ijrmhm.2016.11.004>.
- [3] B. Cheniti, D. Miroud, P. Hvizdoš, J. Balko, R. Sedláč, T. Csanádi, B. Belkessa, M. Fides, Investigation of WC decarburization effect on the microstructure and

- wear behavior of WC-Ni hardfacing under dry and alkaline wet conditions, *Mater. Chem. Phys.* 208 (2018), <https://doi.org/10.1016/j.matchemphys.2018.01.052>.
- [4] H. Hao, Y. Wang, Z. Jin, X. Wang, The effect of interlayer metals on the strength of alumina ceramic and 1Cr18Ni9Ti stainless steel bonding, *J. Mater. Sci.* 30 (1995) 4107–4111, <https://doi.org/10.1007/BF00360716>.
- [5] H. Chen, K. Feng, S. Wei, J. Xiong, Z. Guo, H. Wang, Microstructure and properties of WC-Co / 3Cr13 joints brazed using Ni electroplated interlayer, *RMHM.* 33 (2012) 70–74, <https://doi.org/10.1016/j.ijrmhm.2012.02.018>.
- [6] P.Q. Xu, Dissimilar welding of WC-Co cemented carbide to Ni42Fe50.9Co.6Mn3.5Nb3 invar alloy by laser-tungsten inert gas hybrid welding, *Mater. Design J.* 32 (2011) 229–237, <https://doi.org/10.1016/j.matdes.2010.06.006>.
- [7] H. Chen, K. Feng, J. Xiong, Z. Guo, Characterization and stress relaxation of the functionally graded WC-Co/Ni component/stainless steel joint, *J. Alloys Compd.* 557 (2013) 18–22, <https://doi.org/10.1016/j.jallcom.2012.12.152>.
- [8] H. Chen, K. Feng, S. Wei, J. Xiong, Z. Guo, H. Wang, Microstructure and properties of WC-Co / 3Cr13 joints brazed using Ni electroplated interlayer, *Int. J. Refract. Metals Hard Mater.* 33 (2012) 70–74, <https://doi.org/10.1016/j.ijrmhm.2012.02.018>.
- [9] X. Yin, Q. Ma, B. Cui, L. Zhang, X. Xue, S. Zhong, D. Xu, Current review on the research status of cemented carbide brazing: filler materials and mechanical properties, *Metals Mater. Int.* (2020), <https://doi.org/10.1007/s12540-020-00608-w>.
- [10] Y. Guo, Y. Wang, B. Gao, Z. Shi, Z. Yuan, Rapid diffusion bonding of WC-Co cemented carbide to 40Cr steel with Ni interlayer: effect of surface roughness and interlayer thickness, *Ceram. Int.* 42 (2016) 16729–16737, <https://doi.org/10.1016/j.ceramint.2016.07.145>.
- [11] B. Cheniti, D. Miroud, R. Badji, P. Hvizdoš, M. Fides, T. Csanádi, B. Belkessa, M. Tata, Microstructure and mechanical behavior of dissimilar AISI 304L/WC-Co cermet rotary friction welds, *Mater. Sci. Eng. A* 758 (2019) 36–46, <https://doi.org/10.1016/j.msea.2019.04.081>.
- [12] H. Chen, K. Feng, S. Wei, J. Xiong, Z. Guo, H. Wang, Microstructure and properties of WC-Co/3Cr13 joints brazed using Ni electroplated interlayer, *Int. J. Refract. Met. Hard Mater.* 33 (2012) 70–74, <https://doi.org/10.1016/j.ijrmhm.2012.02.018>.
- [13] M. Amelzadeh, S.E. Mirsalehi, Dissimilar joining of WC-Co to steel by low-temperature brazing, *Mater. Sci. Eng. B Solid-State Mater. Adv. Technol.* 259 (2020) 114597, <https://doi.org/10.1016/j.mseb.2020.114597>.
- [14] M. Amelzadeh, S.E. Mirsalehi, Influence of braze type on microstructure and mechanical behavior of WC-Co/steel dissimilar joints, *J. Manuf. Process.* 36 (2018) 450–458, <https://doi.org/10.1016/j.jmapro.2018.10.015>.
- [15] C. Jiang, H. Chen, Q. Wang, Y. Li, Effect of brazing temperature and holding time on joint properties of induction brazed WC-Co / carbon steel using Ag-based alloy, *J. Mater. Process. Technol.* 229 (2016) 562–569.
- [16] M.N. Avettand-Fènoël, T. Nagaoka, H. Fujii, R. Taillard, Effect of a Ni interlayer on microstructure and mechanical properties of WC-12Co cermet / SC45 steel friction stir welds, *J. Manuf. Process.* 40 (2019) 1–15, <https://doi.org/10.1016/j.jmapro.2019.02.032>.

- [17] K. Feng, H. Chen, J. Xiong, Z. Guo, Investigation on diffusion bonding of functionally graded WC-Co/Ni composite and stainless steel, *Mater. Des.* 46 (2013) 622–626, <https://doi.org/10.1016/j.matdes.2012.11.006>.
- [18] R.U. Vaidya, P. Rangaswamy, M.A.M. Bourke, D.P. Butt, Measurement of bulk residual stresses in molybdenum disilicide/stainless steel joints using neutron scattering, *Acta Mater.* 46 (1998) 2047–2061, [https://doi.org/10.1016/S1359-6454\(97\)00429-1](https://doi.org/10.1016/S1359-6454(97)00429-1).
- [19] D. Travessa, M. Ferrante, G. den Ouden, Diffusion bonding of aluminium oxide to stainless steel using stress relief interlayers, *Mater. Sci. Eng. A* 337 (2002) 287–296, [https://doi.org/10.1016/S0921-5093\(02\)00046-1](https://doi.org/10.1016/S0921-5093(02)00046-1).
- [20] W.C. Oliver, G.M. Pharr, An improved technique for determining hardness and elastic modulus using load and displacement sensing indentation experiments, *J. Mater. Res.* 7 (1992) 1564–1583.
- [21] A. Belyakov, T. Sakai, H. Miura, R. Kaibyshev, K. Tsuzaki, Continuous recrystallization in austenitic stainless steel after large strain deformation 50, 2002, pp. 1547–1557.
- [22] H. Ma, G. Qin, P. Geng, F. Li, B. Fu, X. Meng, Microstructure characterization and properties of carbon steel to stainless steel dissimilar metal joint made by friction welding, *Mater. Des.* 86 (2015) 587–597, <https://doi.org/10.1016/j.matdes.2015.07.068>.
- [23] I. Bhamji, M. Preuss, P.L. Threadgill, R.J. Moat, A.C. Addison, M.J. Peel, Linear friction welding of AISI 316L stainless steel, *Mater. Sci. Eng. A* 528 (2010) 680–690, <https://doi.org/10.1016/j.msea.2010.09.043>.
- [24] P. Hidnert, Thermal expansion of heat-resisting alloys: nickel-chromium, iron-chromium, and nickel-chromium-iron alloys, *Bureau Stand. J. Res.* 7 (1928). [https://nvlpubs.nist.gov/nistpubs/jres/7/jresv7n6p1031\\_a2b.pdf](https://nvlpubs.nist.gov/nistpubs/jres/7/jresv7n6p1031_a2b.pdf).
- [25] K. Mallika, R. Komanduri, Diamond coatings on cemented tungsten carbide tools by low-pressure microwave CVD, *Wear.* 224 (1999) 245–266.
- [26] R.S. Graves, T.G. Kollie, D.L. McElroy, K.E. Gilchrist, The thermal conductivity of AISI 304L stainless steel, *Int. J. Thermophys.* 12 (1991) 409–415, <https://doi.org/10.1007/BF00500761>.
- [27] H. Chen, K. Feng, S. Wei, J. Xiong, Z. Guo, H. Wang, Microstructure and properties of WC-Co / 3Cr13 joints brazed using Ni electroplated interlayer, *Int. J. Refract. Met. Hard Mater.* 33 (2012) 70–74, <https://doi.org/10.1016/j.jrmhm.2012.02.018>.
- [28] A. Fernandez Guillermet, An assessment of the Fe-Ni-W-C phase diagram, *Zeitschrift Fuer Metallkunde/Mater. Res. Adv. Techniq.* 80 (1989) 83–94.
- [29] C.M. Fernandes, A.M.R. Senos, Cemented carbide phase diagrams: a review, *Int. J. Refract. Met. Hard Mater.* 29 (2011) 405–418, <https://doi.org/10.1016/j.jrmhm.2011.02.004>.
- [30] A. Amirasiri, N. Parvin, M.S. Haghshenas, Dissimilar diffusion brazing of WC-Co to AISI 4145 steel using RBCuZn-D interlayer, *J. Manufact. Processes.* 28 (2017) 82–93, <https://doi.org/10.1016/j.jmapro.2017.06.001>.